

Thermal wave propagation in thin films on substrate: the time-harmonic thermal transfer function

Hilmar Straube^{*1}, Otwin Breitenstein¹, and Jan-Martin Wagner^{1,2}

¹Max Planck Institute of Microstructure Physics, Weinberg 2, 06120 Halle, Germany

²Institute of Materials Science, Christian Albrechts University at Kiel, Kaiserstr. 2, 24143 Kiel, Germany

Received 13 January 2011, revised 21 March 2011, accepted 19 April 2011

Published online 27 May 2011

Keywords lock-in thermography, thermal waves, transfer functions, thin films

^{*} Corresponding author: e-mail hstraube@mpi-halle.mpg.de, Phone: +49-345-5582692, Fax: +49-345-5511223

We present an analytical description of thermal wave propagation for cylindrical symmetry based on a transfer function concept which is analogous to optics. This concept leads to a general criterion for the spatial resolution and to computational benefits. It is applied to a medium consisting of a thermally thin layer of highly heat conductive material on a finite substrate. The result is then specialized to the two cases of highly heat conductive layer on quasi-infinite substrate and

finite substrate with no additional layer. This completes the theory of heat propagation between the thermally thick and thermally thin cases. We encounter the mathematical necessity to revise the definition of the latter terms, taking into account the lateral modulation of the thermal signal. The derived expressions are verified experimentally using infrared lock-in thermography.

© 2011 WILEY-VCH Verlag GmbH & Co. KGaA, Weinheim

1 Introduction An oscillating heat source in or on a solid sample leads to a so-called thermal wave [1], which is the basis of a variety of measurement and imaging methods [2]. The thermal wave patterns are analyzed in order to determine thermal and optical properties of materials such as their absorption, conductivity, diffusivity, effusivity or heat capacity using the photoacoustic method [3] and related photothermal techniques like photothermal beam deflection (for a review, see Ref. [4]), photothermal surface displacement [5, 6], the 3ω method [7, 8] or the recently developed frequency-domain thermoreflectance method [9, 10]. Other properties are also accessible such as elastic anisotropy [11], nonlinear optical surface [12] or magnetocaloric [13] properties. In addition, various thermal-wave imaging methods have been developed such as scanning photoacoustic microscopy [14], photothermal [15, 16] and thermoreflectance [17–19] microscopy as well as lock-in thermography (LIT) [20–22]. Thermal wave-based measurement and imaging methods are used in a broad area of applications, ranging from non-destructive evaluation (NDE) of materials [23, 24], biological and medical investigations [25, 26], testing of electronic devices [27], to materials research (see, e.g., [28]), with a resolution reaching down to the micro- and nanoscale [29–31].

Thermal waves are a special type of diffusive waves [32, 33] and, as such, are strongly damped. Both their wavelength and damping are determined by the thermal diffusion length $\Lambda = \sqrt{2D/\omega}$, with the thermal diffusivity D and the angular frequency ω of the thermal wave in a homogeneous medium [1, 34]. Analogously to optical penetration and considering only one-dimensional heat propagation, a medium is usually considered to be thermally thin (thick) if, for a given frequency, its thickness is much smaller (much larger) than Λ (see, e.g., [3]). In layered systems there are several diffusion lengths corresponding to the different materials. Therefore, such systems show a strong dependency on the excitation frequency due to the varying penetration depth. Film-on-substrate systems have been given special attention, where thermal wave investigations aimed, on the one hand, at determining certain material parameters (as, e.g., film thickness [6, 35], thermal conductivity, diffusivity or effusivity [36–38], thermal interface resistance [39], or several of these together [10, 40, 41]), on the other hand, at the investigation of fundamental aspects of heat transport (as, e.g., in amorphous [42–44] or alloyed [45] materials).

Mathematically, thermal waves are obtained as solutions of the heat equation under certain boundary conditions and

for various source terms. A universally applicable solution is the Green's function obtained as the thermal response to a point-like excitation, also called the point spread function (PSF). Appropriate solutions (either analytical or numerical) are needed to quantitatively evaluate the measurements in terms of various material properties or to deconvolute images of subsurface heat sources or inhomogeneities/defects.

Here, we present an analytical approach to the heat conduction problem with cylindrical symmetry, making thoroughly use of the physical and mathematical properties of the functions involved. We apply a Hankel transform to find the PSF in terms of (lateral) spatial frequencies. This Hankel-transformed PSF turns out to be identical to a transfer function in the same way as it is known from optics, therefore we call it the thermal transfer function (TTF). Using the TTF has several advantages: analytical solutions for the TTF can be found for cases where the PSF cannot be determined explicitly, it is computationally more efficient to use the TTF for determining the resulting temperature signal than to convolute the source distribution with the PSF, and the TTF provides a well-defined criterion for the lateral resolution of the thermal imaging process it describes. By choosing suitable dimensionless variables, this resolution criterion can be generalized to arbitrary material combinations, providing a universal description of the transition from thermally thin to thermally thick behaviour. We encounter the mathematical necessity to revise the definition of the latter terms, taking into account the lateral modulation of the thermal signal.

As a prototypical case of a layer-on-substrate system, we derive the TTF for a thermally thin but highly heat conductive layer on a substrate whose *finite* thickness has to be taken into account; solutions for several other cases are derived as limiting cases (*cf.* Fig. 1). Although the mathematical expression needed to treat such a layer (the latter being abbreviated as HCL in the following) as a special boundary condition is already discussed in the famous book by Carslaw and Jaeger [1], surprisingly, no rigorous solution of the heat equation for this case is found in the literature. Maznev et al. [46] as well as Hartmann et al. [18] used the HCL boundary condition for a semi-infinite substrate, but implicitly together with a certain random, unrealistic heat source distribution just suited for obtaining a simple dispersion relation for the thermal waves. Cole [47, 48] used a boundary condition for a thin film that only comprises its heat capacity but disregards the lateral thermal conductivity inside the thin film.

Instead of a HCL boundary condition a highly heat conductive layer of finite thickness can be used in the theoretical description of such a system. This was done, *e.g.*, by Reichling and Grönbeck [49], who even treated a double layer on the surface of a semi-infinite substrate. However, assuming a surface excitation by a Gaussian laser beam they obtained quite complex expressions that cannot easily be used for general purposes, and although their solutions include the lateral dependency, this is neither displayed nor discussed in the remainder of their work. In contrast,

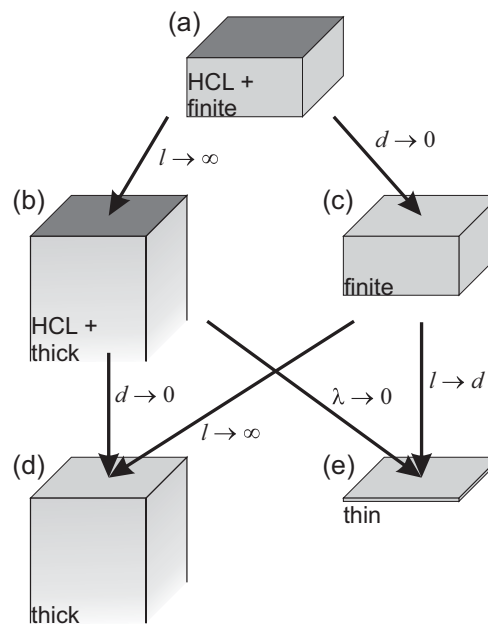


Figure 1 Cases of heat propagation treated in this contribution. (a) HCL on a finite substrate, (b) ditto on a thermally thick substrate, (c) finite thickness sample, (d) thermally thick sample, (e) thermally thin sample. Since (a) is the most general case, the others can be found as limiting cases as indicated on the arrows (d layer thickness, l substrate thickness, λ substrate heat conductivity).

Frétygné et al. [19] explicitly discuss the lateral dependency of the thermal signal using a general expression for a film-on-substrate system and an arbitrary excitation shape. However, both their results have two limitations, being inherently present in their integral kernels: they are restricted to excitation and detection at the surface, and a semi-infinite substrate is assumed. No such restrictions are present in our solutions.

2 Theory

2.1 PSF solution of the heat equation

2.1.1 Geometry and heat equation The geometry and coordinate system are shown in Fig. 2. The upper surface is assumed at $z = 0$ and the source at $z' \geq 0$ below the surface. In the case of a finite thickness substrate [Fig. 1(a) and (c)] the back surface is at $z = l$, $0 \leq z' \leq l$, for thermally thick substrates [Fig. 1(b) and (d)] it is assumed to be at $z = \infty$. The highly heat conductive layer at $z = 0$ of thickness d is assumed to be thermally thin.

A point source $q_P = \delta^3(\mathbf{r} - \mathbf{r}_0)$ oscillates at \mathbf{r}_0 ($r = 0$, $z = z'$) with excitation angular frequency ω and unit amplitude. The temperature response P to this point-like source is described by the point spread function (PSF). For our purposes (excitation frequency smaller than the inverse of the lifetime of heat-carrying phonons), it is obtained from the parabolic heat equation, written as

$$-\frac{q_P e^{i\omega t}}{\lambda} = \Delta P(r, z) e^{i\omega t} - \frac{1}{D} \frac{\partial}{\partial t} [P(r, z) e^{i\omega t}], \quad (1)$$

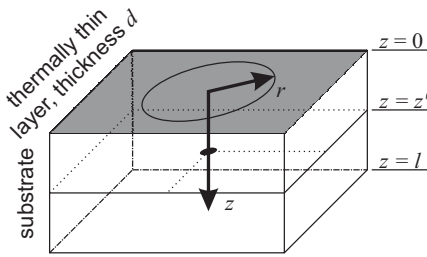


Figure 2 Geometrical conventions. The substrate of thickness l is covered with a thermally thin layer of thickness d such that temperature variations in z -direction inside the thin layer can be neglected. Because of the cylindrical symmetry, no polar angle φ is needed. The source is centred at $r = 0$, depth z' .

where the three-dimensional Laplace operator is denoted by Δ and $D = \lambda/c_p\rho$ is the thermal diffusivity with the thermal conductivity λ , specific heat c_p and density ρ . The constants in Eq. (1) are chosen such that the PSF receives the unit K/W to reflect its meaning as the temperature profile for a point source of unit power. Other conventions used in literature [1, 47, 48, 50] can be traced back to different constants in the heat equation.

Both source and temperature response have a time dependency of the form $e^{i\omega t}$, which cancels from Eq. (1). A phase shift between source and response is fully expressed by the argument of the complex-valued function P . Thus the equation to be solved is

$$-\frac{q_P}{\lambda} = \Delta P(r, z) - \frac{i\omega}{D} P(r, z). \quad (2)$$

2.1.2 Boundary conditions The boundary conditions to the heat equation (2) describe the nature of the surfaces and how (if at all) heat is exchanged with the environment. Heat transfer from the medium to the environment can occur via radiation, conduction and convection. In most contributions, the effect of heat loss is tacitly neglected. Some authors made efforts to introduce it into the functional form of the PSFs [32, 47, 48]. However, to actually be able to predict heat loss behaviour, it is necessary to consider surface emissivity variations for radiation, to measure the thermal contact resistance of conduction to the sample holder and to solve the Navier–Stokes equation in air coupled to the time-harmonic heating in the medium for convective heat loss, as pointed out by Rousset et al. [51]. Therefore, it is either necessary to deal with a significant complication of both theory and experiment to correctly describe heat loss behaviour or to move to a regime where it is negligible. In the following we will assume the latter, a condition that has been termed ‘quasi-adiabatic’ ($\partial P/\partial z = 0$ at the surfaces) and can be verified experimentally [22] and theoretically [52].

The HCL boundary condition needed for cases (a) and (b) is a little more complicated than the simple adiabatic

boundary condition for the other surfaces. The highly heat conductive layer on the surface is assumed to be thermally thin, the heat conduction in the layer is essentially two-dimensional (cf. § 1.9 H in Carslaw–Jaeger [1]) according to

$$\Delta_2 P(r, 0) + h \frac{\partial P}{\partial z}(r, 0) - \frac{i\omega}{D_f} P(r, 0) = 0, \quad (3)$$

where Δ_2 is the planar Laplace operator, $h\partial P(r, 0)/\partial z$ describes the heat flux ($-\lambda\nabla T|_{z=0}$) between substrate and layer (assuming zero thermal resistivity between layer and substrate)¹, and $h = \lambda/d\lambda_f$. Index f refers to properties of the thin film² of thickness d . This equation describes the heat conduction in the layer and (implicitly) that no heat is transferred to the environment and serves thus both as the heat equation in the thin material and the quasi-adiabatic boundary condition for the system at $z=0$. Note that through the HCL boundary condition (3) a second thermal diffusion length Λ_f is introduced. Therefore, the thermal diffusion length Λ of the substrate fails to be useful as a characteristic length of the thermal waves in the presence of a highly heat conductive layer. We will come back to this issue in Section 3.3.1.

For a thin layer with a thermal conductivity close to that of the substrate, the influence of the ‘highly heat conductive layer’ becomes negligible. If it is lower than that of the substrate, a temperature drop normal to the layer will develop, the thin layer will no longer be *thermally thin*, and cannot be described appropriately by Eq. (3). Its behaviour is then that of a thermal resistance.

2.1.3 Reduction to ordinary differential equation and solution with inhomogeneity

The partial differential equation (2) can be reduced to an ordinary differential equation by a two-dimensional spatial Fourier transform (denoted by a tilde; $x \rightarrow k_x, y \rightarrow k_y, k^2 = k_x^2 + k_y^2$). In the present case of cylindrical symmetry, it takes the form of the Hankel transform of order zero [54]:

$$\tilde{P}(k, z) = \mathcal{F}_{2-d}[P(r, z)] = \mathcal{H}_0[P(r, z)]. \quad (4)$$

The heat equation (2) transforms into an ordinary differential equation [54] according to $\Delta = \Delta_2 + \partial^2/\partial z^2 \rightarrow -k^2 + \partial^2/\partial z^2$:

$$-\frac{\tilde{q}_P}{\lambda} = -\eta^2 \tilde{P}(k, z) + \frac{\partial^2 \tilde{P}(k, z)}{\partial z^2}, \quad (5)$$

¹ Whether a (Kapitza-type) interfacial thermal resistance between HCL and substrate influences the heat transport to the substrate depends on the excitation frequency. The substrate layer affected by the thermal wave has a thickness of $\Lambda \propto \omega^{-1/2}$ and a corresponding thermal resistance $R_\Lambda = \Lambda/\lambda$. The interface resistance R is negligible as long as $R \ll R_\Lambda$. Typical values for R can be found in Ref. [53].

² In the case of a thermally thin layer whose thermal properties vary along the z -axis, the straightforward substitutions $h = \lambda/d\lambda_f \rightarrow \lambda/\int_z \lambda_f(z) dz$ and $D_f = c_{p,f}\rho_f/\lambda_f \rightarrow \int_z c_{p,f}(z)\rho_f(z) dz/\int_z \lambda_f(z) dz$ are appropriate.

using the notation³

$$\eta = \sqrt{k^2 + \frac{i\omega}{D}} = \sqrt{k^2 + \frac{2i}{\Lambda^2}}. \quad (6)$$

This term occurs naturally when dealing with the Fourier transformed, time-harmonic heat equation. With the introduction of η , the transformed heat equation (5) shows the mathematical form of a one-dimensional wave equation in z -direction, where η takes the place of the wave vector. Since η depends on k , the wave propagation and damping in z -direction depends on the spatial frequency in radial direction.

The transformation of the HCL boundary condition (3) yields

$$-\eta_f^2 \tilde{P}(k, 0) + h \frac{\partial \tilde{P}(k, 0)}{\partial z} = 0, \quad (7)$$

where the formal analogue $\eta_f = \sqrt{k^2 + i\omega/D_f}$ is introduced. Note that the equation describing heat transfer inside the thin layer takes the form of a boundary condition of the third kind in Fourier space.

To solve the heat conduction problem its (unknown) solution is split into two parts $P = u + w$, where w solves the homogeneous heat equation with free parameters and u is the solution of the full heat equation (including the source term) in an infinite medium (no surfaces). The problem is solved if the free parameters in w are adjusted such that P satisfies the boundary conditions. The equation for $\tilde{w}(k, z)$, $0 = -\eta^2 \tilde{w}(k, z) + \partial^2 \tilde{w}(k, z) / \partial z^2$, is solved by $\tilde{w}(k, z) = A(k) \exp(-\eta z) + B(k) \exp(\eta z)$ with the free parameters $A(k)$ and $B(k)$. The function $u(r, z)$, the Green's function of an oscillating point source in an infinite medium, is known to be (cf. § 10.4 VI in Carslaw–Jaeger [1])

$$u(r, z) = \frac{1}{4\pi\lambda} \frac{\exp\left(-\sqrt{i\omega[r^2 + (z - z')^2]/D}\right)}{\sqrt{r^2 + (z - z')^2}}, \quad (8)$$

which has a simple Hankel transform:⁴

$$\tilde{u}(k, z) = \frac{1}{2\lambda} \frac{\exp(-\eta|z' - z|)}{\eta}. \quad (9)$$

If the PSF solution is actually needed in real space, the inverse Hankel transform of $\tilde{P}(k, z) = \tilde{u}(k, z) + \tilde{w}(k, z)$ can be found numerically by a standard two-dimensional fast Fourier transform or by specialized algorithms that make use of the radial symmetry. For most applications, however,

the transformed PSF is more useful in itself as will be detailed in the following Section 2.2.

A rather general but less direct approach can also be followed to obtain the PSF. If the solution of the corresponding one-dimensional problem is known, *i.e.*, the thermal wave solution for a source that is homogeneous in the x - y plane, the PSF can be obtained by replacing the expression $i\omega/D(z)$ in the one-dimensional solution of the heat equation by $\eta^2(z) = i\omega/D(z) + k^2$ and performing the inverse Hankel transform, as shown in the book of Mandelis [32], theorem 5.1. The case of a HCL is not present in Mandelis' treatment. In fact, following this procedure in the presence of a HCL does not lead to the desired solution as essential terms cancel.

2.2 Point spread function (PSF), line spread function (LSF), and thermal transfer function (TTF)

The point spread function (PSF), $P(r, z)$, is closely related to two other functions that describe the response of a system to thermal excitation. These are the line spread function (LSF), $L(x, z)$ and the thermal transfer function (TTF), $F(k, z)$. They describe the response to different kinds of heat sources, visualized in Fig. 3. While the PSF is the thermal wave response to a point-like heat source at the source position \mathbf{r}_0 ($r = 0, z = z'$), the LSF is the response to a line heating source parallel to the surface at $z = z', x = 0$ (without loss of generality). The concept of the TTF is borrowed from optics [56] where it appears as the (complex) optical transfer function (OTF). It can be defined through integral transformations of the PSF and LSF [57]. (We will discuss its meaning in real space in Section 2.2.2 below.)

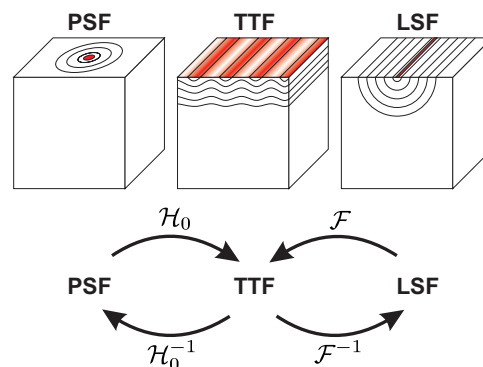


Figure 3 (online colour at: www.pss-b.com) Relationship between PSF, TTF and LSF. Heat sources and thermal waves related to the three functions are illustrated for a thermally thick medium. The heating power density is shown as a red surface quantity, solid curves indicate the resulting thermal wave fronts. As the TTF is defined in Fourier space only, the image shows its effect on a single Fourier component in real space, see Section 2.2.2. In the case of radial symmetry of the PSF, all three functions contain the same information and can be calculated from each other using Hankel (\mathcal{H}_0) and Fourier (\mathcal{F}) transforms.

³ Here and henceforth the expression \sqrt{c} with a complex number c denotes the principal value of the square root, *i.e.*, $\sqrt{c} = \sqrt{\rho} \exp(i\phi) = \sqrt{\rho} \exp(i\phi/2)$, with $-\pi < \phi \leq \pi$.

⁴ This is found by evaluating a variant of Sonine's second integral, see Ref. [55], § 13.47, Eq. (2), setting $\mu \rightarrow 0, \nu \rightarrow 1/2, t \rightarrow r, b \rightarrow k, z \rightarrow z - z'$ and $a \rightarrow \sqrt{i\omega/D}$.

It holds that

$$F(k, z) = \mathcal{F}[L(x, z)] = \int_{-\infty}^{\infty} L(x, z) \exp(-ixk) dx, \quad (10a)$$

$$L(x, z) = \mathcal{F}^{-1}[F(k, z)] = \frac{1}{2\pi} \int_{-\infty}^{\infty} F(k, z) \exp(ixk) dk, \quad (10b)$$

$$F(k, z) = \mathcal{H}_0[P(r, z)] = 2\pi \int_0^{\infty} P(r, z) J_0(rk) r dr, \quad (10c)$$

$$P(r, z) = \mathcal{H}_0^{-1}[F(k, z)] = \frac{1}{2\pi} \int_0^{\infty} F(k, z) J_0(rk) k dk. \quad (10d)$$

(J_0 is the Bessel function of the first kind of order zero.)

From Eqs. (10a–d) it is clear that PSF/TTF is a Hankel transform pair in r/k and LSF/TTF a Fourier transform pair in x/k . Comparing Eq. (4) to (10c) it is also apparent that \tilde{P} from Section 2.1 is the TTF:

$$\tilde{P}(k, z) \equiv F(k, z). \quad (11)$$

In addition to the Fourier and Hankel transform formulas involving the TTF above, it is also possible to calculate the LSF directly from the PSF in a straightforward way (even *vice versa* [57, 58]):

$$L(x, z) = \int_{-\infty}^{\infty} P(\sqrt{x^2 + y^2}, z) dy = 2 \int_x^{\infty} \frac{P(r, z) r}{\sqrt{r^2 - x^2}} dr. \quad (12)$$

No information is lost through these integral transforms; PSF, TTF and LSF all contain the same information.

2.2.1 Convolution and deconvolution In order to understand the meaning of the TTF consider the case of a planar heat source $Q(x, y)$ (given in Wm^{-2}). Then, the corresponding temperature field at depth z is obtained from the two-dimensional convolution integral of the PSF $P(r, z)$ with $Q(x, y)$, both at depth z' :

$$T_m(x, y, z) = \iint P(r', z) Q(x - x', y - y') dx' dy' = P(r, z) * Q(x, y), \quad (13)$$

with $r = \sqrt{x^2 + y^2}$. By the convolution theorem [54], this convolution corresponds to a multiplication in Fourier space. The two-dimensional Fourier transform of the PSF is the TTF, Eq. (14), and the Fourier transform of the source power distribution \tilde{Q} needs to be calculated numerically for

most cases (with the important exception of Gauss profiles):

$$\tilde{T}_m(k_x, k_y, z) = F(k, z) \tilde{Q}(k_x, k_y). \quad (14)$$

For all cases except simple ‘thermally thin’ and ‘thermally thick’, only the TTF (but not the PSF and LSF) can be found as a simple expression (see Section 3.2). However, calculating the convolution via two Fast Fourier Transforms and a simple multiplication (14) is computationally more efficient [59] than the direct calculation following (13) [$O(N \log N)$ vs. $O(N^2)$]. Deconvolution procedures like Wiener optimal filtering [59] also operate in Fourier space. Thus, it is actually fortunate that simple analytical expressions are found for the TTF and not the PSF and LSF in Section 3 below.

2.2.2 The TTF in real space Until now, the TTF was only introduced as the Hankel transform of the PSF (*i.e.*, the two-dimensional Fourier transform in the x – y plane) and the Fourier transform of the LSF. We shall now describe its physical meaning in real space.

The Fourier transform of the heat source distribution $Q(x, y)$ (at depth z') decomposes the source into its spatial frequency components. If we pick one at a certain spatial frequency vector $\mathbf{k} = (k_x, k_y)$ it corresponds to

$$Q_{\mathbf{k}}(x, y) = a \exp[i(k_x x + k_y y)], \quad a = \frac{\tilde{Q}(k_x, k_y)}{4\pi} dk_x dk_y, \quad (15)$$

in real space (heating in Wm^{-2} at depth z'). Due to the linearity of the system and as described by the convolution theorem (14) this Fourier component of the heating source causes a temperature response at the same spatial frequency \mathbf{k} :

$$T_{\mathbf{k}}(x, y, z) = F(\mathbf{k}, z) Q_{\mathbf{k}}(x, y). \quad (16)$$

This means that the absolute value and argument of the (complex-valued) TTF $F(\mathbf{k}, z)$ for a given spatial frequency vector \mathbf{k} at observation depth z is the response-to-excitation modulation amplitude ratio and phase shift, respectively. The thermal wave pattern $T_{\mathbf{k}}(x, y, z)$ that results from the heat source $Q_{\mathbf{k}}(x, y)$ at $z' = 0$ is shown in Fig. 3 to illustrate this real-space meaning of the TTF. The thermal response for the important limiting case of homogeneous planar excitation can be calculated easily from the TTF since this can be viewed as an excitation of spatial frequency $\mathbf{k} = 0$.

Since the TTF for a given spatial frequency is a complex number, it causes a phase shift between the sinusoidal heating pattern $Q_{\mathbf{k}}(x, y)$ and the thermal response $T_{\mathbf{k}}(x, y, z)$. This phase shift can be thought of as a spatial shift in the x – y plane between excitation and response patterns or as a temporal shift; both views are mathematically equivalent. This ambiguity in the real-space meaning does not occur for the PSF (and LSF). There the argument of the complex-valued function is clearly the time-lag between excitation and the thermal response at the observation point.

Table 1 TTFs for cases (a) through (e) in Fig. 1.

Case	$F(k, z)^a$	$F(k)^b$
(a) HCL on finite substrate	$\frac{\cosh \eta(l-z') \eta_f^2 \sinh \eta z + h \eta \cosh \eta z}{\lambda \eta \frac{\eta_f^2 \cosh \eta l + h \eta \sinh \eta l}{\eta_f^2}}$	$\frac{1}{\lambda \eta_f^2 \cosh \eta l + h \eta \sinh \eta l} h \cosh \eta l$
(b) HCL on thermally thick	$\frac{e^{-\eta z'} \eta_f^2 \sinh \eta z + h \eta \cosh \eta z}{\lambda \eta \frac{\eta_f^2 + h \eta}{\eta_f^2}}$	$\frac{1}{\lambda \eta_f^2 / h + \eta} 1$
(c) finite substrate	$\frac{\cosh \eta(l-z') \cosh \eta z}{\lambda \eta \frac{\sinh \eta l}{\eta_f^2}}$	$\frac{1}{\lambda \eta} \coth \eta l$
(d) thermally thick	$\frac{\exp(-\eta z') \cosh \eta z}{\lambda \eta}$	$\frac{1}{\lambda \eta}$
(e) thermally thin	–	$\frac{1}{d \lambda_f \eta_f^2}$

^aGiven for observation above source ($z \leq z'$), z and z' change place for $z > z'$. ^b $F(k, z)$ for $z = z' = 0$.

There are two main differences in the application of the transfer function concept to the heat conduction problem and its use in optics. Firstly, in optics for incoherent illumination, phase information is unimportant and only the real-valued modulation transfer function (MTF) needs to be considered, while the phase information in the TTF is essential. Another important difference is that for the MTF in optics both source and image are intensity functions whereas for the TTF the source is a power density distribution in units of Wm^{-2} and the image a temperature distribution in units of K. Therefore, the MTF is dimensionless and the TTF has the dimension Km^2W^{-1} .

A thermal analogue of such an MTF was introduced in the context of pulsed thermography by Shepard et al. [60, 61] and Krapez [62] as the temperature or image contrast obtained from a resolution test object. Another transfer function approach was proposed by Mandelis [63]. Designed for photothermal-wave diffraction, his thermal-wave transfer function relates the (complex) temperature distributions at the aperture plane and at the observation plane; thus, this type of transfer function is dimensionless like the MTF.

3 Results

3.1 Transfer function results It is possible to calculate the TTFs for cases (a) through (e) following the procedure outlined in the previous section for each case. It is, however, more efficient to start with the mathematically most complex case (a) and specialize the result as limiting cases according to the arrows in Fig. 1; results are given in Table 1. An important special case is that of a source on top of the sample (or inside the thin layer covering the sample) and of a temperature modulation signal observed at the topmost layer. Then $z' = z = 0$ and the expressions simplify considerably, these TTFs are also given in the table. Using the expressions from Table 1 together with the integral transforms (10a) through (10d), a large subset of thermal wave experiments can be modelled conveniently.

Performing the limits to thermally thin or thermally thick behaviour ($l \rightarrow d$, $l \rightarrow \infty$ in Fig. 1) it is found that the thermally thin approximation is approached only if $|\eta l| \ll 1$. It is not approached if the layer is just thin compared to the

thermal diffusion length, $l/\Lambda \ll 1$. Similarly, the thermally thick approximation is found for $|\eta l| \gg 1$.⁵ Through the term η , these expressions depend on the lateral modulation with spatial frequency $k = 2\pi/s$, where s represents the feature size that is evaluated,

$$\eta l = \left[2i \left(\frac{l}{\Lambda} \right)^2 + 4\pi^2 \left(\frac{l}{s} \right)^2 \right]^{1/2}. \quad (17)$$

The requirement $|\eta l| \ll 1$ for thermally thin behaviour consists thus of two necessary conditions. The first condition is the classical definition of the term: a thermally thin layer is much thinner than the thermal diffusion length in the material, $l/\Lambda \ll 1$. This condition is not sufficient for inhomogeneous heating, ηl is not negligibly small if highly detailed samples are investigated (corresponding to high spatial frequency components). Therefore in addition to $l/\Lambda \ll 1$ also $l/s \ll 1$ needs to be given for thermally thin approximations to be valid. As an illustration of this condition consider a point-like heat source on top of a $l = 0.2$ mm thick silicon wafer at an excitation frequency of 1 Hz. The thermal diffusion length is $\Lambda = 5.4$ mm, such that the condition $l \ll \Lambda$ is well satisfied. Obviously though, the resulting temperature field closer than 0.2 mm to the point source will not be 'essentially two-dimensional' as supposed by the thermally thin approximation. The temperature field at a distance from the point source large compared to the thickness, in contrast, is well described by the thermally thin approximation, *i.e.*, neglecting the z -dependency of the temperature field. Thus, the question is not whether a sample is thermally thin at a certain excitation frequency but rather if all relevant spatial frequency components of the signal can be described sufficiently well by assuming the sample to be thermally thin.

The same reasoning leads to an extension of the traditional definition of 'thermally thick'. Thermally thick

⁵ Both conditions can be seen most clearly in the limits from case (c) to cases (d) and (e).

behaviour is not only present if $l \gg \Lambda$ but also if very small features are under investigation.

The case of a slab of finite thickness (c) given in the table was already treated by several authors [22, 32, 47, 48, 50]. These discussions are based on the argument of mirror heat sources (cf. § 10.10 in Carslaw–Jaeger [1]) in real space that leads to an infinite sum of terms in the form of Eq. (8). Compared to this infinite sum, using the expression for the TTF in Fourier space is obviously computationally advantageous. The expression for $F(k)$ of case (c) given in the table was already used implicitly by Salazar et al. [64] to arrive at their formula for the response to a Gaussian beam heating a finite thickness sample (given in Appendix A of their contribution). The case of a highly heat conductive layer of finite thickness on a thermally thick substrate and for $z = z' = 0$ was treated by Frétiigny et al. [19], using a different convention for the units. It can be easily shown that their integral kernel \bar{T} converges to our expression for $F(k)$ of case (b) in the limit of thermally thin behaviour of the layer.

3.2 Explicit results for the PSF and LSF for the thermally thin and thick cases Explicit expressions for PSF and LSF are possible for thermally thin and thermally thick homogeneous media. These expressions are widely used in the literature and are given here for completeness. In all other cases, simple analytical expressions are only found for the TTF. In case the evaluation cannot be done in the Fourier domain, the inverse transform to PSF and LSF according to Eqs. (10) b and d has to be done numerically.

For the thermally thin case (e) one has an integral of Hankel type (cf. § 13.51, Eq. (5) in Ref. [55]):

$$P_e(r) = \frac{1}{2\pi d\lambda_f} \int_0^\infty \frac{kJ_0(rk)}{\eta_f^2} dk \quad (18)$$

$$= \frac{1}{2\pi d\lambda_f} K_0\left(r\sqrt{\frac{i\omega}{D_f}}\right),$$

with the modified Bessel function of second kind and order zero K_0 . For the thermally thick case (d) the integral can be solved applying the relation already used for Eqs. (8), (9):

$$P_d(r, z) = \frac{1}{2\pi} \int_0^\infty \frac{e^{-\eta z'}}{2\lambda\eta} (e^{\eta z} + e^{-\eta z}) kJ_0(rk) dk$$

$$= \frac{\exp\left[-\sqrt{i\omega[r^2 + (z - z')^2]/D}\right]}{4\pi\lambda\sqrt{r^2 + (z - z')^2}} \quad (19)$$

$$+ \frac{\exp\left[-\sqrt{i\omega[r^2 + (z + z')^2]/D}\right]}{4\pi\lambda\sqrt{r^2 + (z + z')^2}}.$$

(Given for $z \leq z'$; switch z and z' for $z' < z$.) The two terms in Eq. (19) can be interpreted as the source at z' and its ‘mirror heat source’, reflected at the sample surface to satisfy the boundary condition $\partial P/\partial z(r, 0) = 0$, cf. § 10.10

in Carslaw–Jaeger [1]. The expressions (18) and (19) are well-known and given, e.g., by Breitenstein et al. [22] and by Mandelis [50] (called three-dimensional semi-infinite and two-dimensional Green’s function there, using a different convention for the unit of the PSF).

The expressions for the LSFs are

$$L_e(x) = \frac{1}{2d\lambda_f\sqrt{i\omega/D_f}} \exp\left(-|x|\sqrt{\frac{i\omega}{D_f}}\right) \quad (20)$$

for the thermally thin case (e) and

$$L_d(x, z) = \frac{1}{2\pi\lambda} K_0\left(\sqrt{\frac{i\omega[x^2 + (z' - z)^2]}{D}}\right) \quad (21)$$

$$+ \frac{1}{2\pi\lambda} K_0\left(\sqrt{\frac{i\omega[x^2 + (z' + z)^2]}{D}}\right)$$

for the thermally thick case (d). The line heating source is assumed at the line $x = 0$ in both cases. This agrees with expressions found in literature (e.g., in a contribution by Cole [47, 48], using a different convention for the unit of the LSF). The similarity between the LSF in a thick medium (21) and the PSF in a thin medium (18) is no coincidence as both problems are two-dimensional [22, 50]. Similarly, the LSF for the thermally thin case (20) is the solution to a one-dimensional problem and corresponds to the propagation of a planar thermal wave into a semi-infinite medium [1].

3.3 Spatial resolution and phase

3.3.1 Spatial resolution The temperature profile in the detection plane resulting from periodic excitation of a sample follows the lateral heating power distribution. Thus the temperature profile in the detection plane can be seen as a blurred image of this heating power density. When this temperature profile is mapped using any method, e.g., an IR camera or a scanning temperature sensor, the image of the power distribution will be blurred again.

Therefore, the step from the heating power distribution to the temperature profile (calculated using the TTF) may be viewed as the first in a series of imaging steps (each with a characteristic transfer function) from the source to the measured signal, where in each step a certain amount of information about the lateral heating power distribution is lost. In many cases, this loss of detail is dominant for the very first step, i.e., the resolution in imaging the heat source is most significantly lowered through heat conduction in the sample from the heat source to the surrounding material.

In combined systems of highly heat conductive layer and substrate, the traditional way of assessing the lateral resolution of the temperature profile with the thermal diffusion length [22] is no longer valid. This is because these systems have two different thermal diffusion lengths, Λ of the substrate and Λ_f of the film, which may differ

considerably. Another resolution criterion for these systems is thus needed.

The heat generation in a sample may contain very high spatial frequencies. For example a short circuit in an electrical device produces heat very locally (diameters typically less than $10\ \mu\text{m}$). The high spatial frequencies associated with such a source are not present in the thermal signal. This is because the TTF acts as a low-pass filter that filters out high spatial frequency components (*i.e.*, information about details).

The cutoff (spatial) frequency of the TTF thus gives a convenient resolution criterion if the resolution is in fact limited by the spreading of heat. Here we follow the usual convention of defining the cutoff frequency k_c as the frequency where the amplitude has dropped to $1/\sqrt{2}$ of its value for homogeneous excitation ($k=0$), corresponding to an attenuation of 3 dB:

$$\begin{aligned} |F(k_c)| &= |F(0)|/\sqrt{2}, \\ s_c &= 2\pi/k_c. \end{aligned} \quad (22)$$

That means a resolution test object with heater lines with a line-to-line spacing of s_c will show a temperature contrast which is a factor of $1/\sqrt{2} \approx 0.71$ worse than for a spacing of $s \gg s_c$. This cutoff wavelength s_c is proposed as a measure of the lateral resolution of the data about the heat sources in the temperature field.

For NDE applications, apart from the geometry of a defect, its depth is of particular interest. It is found that the phase signal carries most information about the depth [23]. A theoretical treatment of the achievable depth resolution, however, is beyond the scope of this contribution.

The proposed criterion for the lateral resolution in thermal imaging can be compared to the thermal diffusion length in the thermally thick case (d), and thermally thin case (e), see Table 1, by solving the resolution equation (22) for s_c and substituting the thermal diffusion length:

$$s_c^{\text{thick}} = \sqrt[4]{\frac{4}{3}}\pi\Lambda \approx 3.38\Lambda, \quad (23)$$

$$s_c^{\text{thin}} = \sqrt{2}\pi\Lambda \approx 4.44\Lambda. \quad (24)$$

The resulting s_c is directly proportional to the thermal diffusion length but with differing factors for the two cases. Hence in two samples of the same material, one thermally thick, the other thermally thin, the resolution will be assessed to be slightly better on the thermally thick sample by the cutoff frequency criterion. For all the other cases (22) has to be solved numerically, which is a simple task for today's computers.

The value of the cutoff wavelength s_c might also serve as a replacement of the thermal diffusion length as a characteristic length of the temperature field in radial direction, just as the thermal diffusion length in a homogeneous medium is useful both as a characteristic dimension of thermal waves and as a resolution criterion for

imaging heat sources through the temperature modulation field.

As an illustrative example for the proposed resolution criterion, consider the silicon on glass structure investigated in the experimental Section 4.1 below. It is essentially a $1.5\ \mu\text{m}$ thick fully (poly-)crystalline silicon film on a thick borosilicate glass substrate (which differ in thermal diffusion length by a factor of 12). Figure 4 shows its (complex) TTF for an excitation frequency of 10 Hz; heat source and signal observation at the surface. Also the derived cutoff frequency is shown. As expected, the corresponding resolution of the combined system $s_c = 1.4\ \text{mm}$ is between that of the silicon alone ($s_c^{\text{thin}} = 7.8\ \text{mm}$) and that of the glass alone ($s_c^{\text{thick}} = 0.5\ \text{mm}$).

Figure 5(a) shows the frequency dependence of the resolution parameter s_c in the silicon on glass system compared to that of heat propagation in the thermally thick glass and in the silicon layer, respectively, as if these were not coupled. It can be seen that the system approaches thermally thin behaviour for very high frequencies (as the penetration depth into the glass diminishes) and thermally thick behaviour for very low frequencies. In the transition region, the slope of the curve is less steep than that of those for both thermally thin and thermally thick approximations. In the double logarithmic plot, the slope is $\approx -1/4$ compared to $-1/2$ of both limiting cases. That means that in this transition region doubling the excitation frequency improves the resolution not by a factor of $2^{1/2} \approx 1.41$ but only of $2^{1/4} \approx 1.19$. A generalized version of this plot is possible and will be described in Section 3.3.3.

A graph similar to Fig. 5(a) was derived by Maznev et al. [46] considering a HCL on a thermally thick substrate. They solved the heat equation using an ansatz that corresponds implicitly to a certain arbitrary heat source distribution in the y - z plane. Then they interpret a term in the resulting solution as a horizontal wave number, which gives a characteristic length of horizontal heat propagation. Although this characteristic length shows a qualitatively similar behaviour to s_c , the generality of their approach remains questionable.

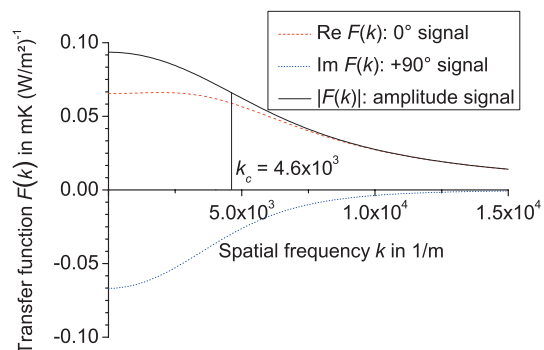


Figure 4 (online colour at: www.pss-b.com) Complex TTF for a system of $1.5\ \mu\text{m}$ silicon on a thick glass substrate at 10 Hz. The cutoff spatial frequency of k_c of this system corresponds to a resolution of $s_c = 1.4\ \text{mm}$. (Heat source and signal observation at the surface.)

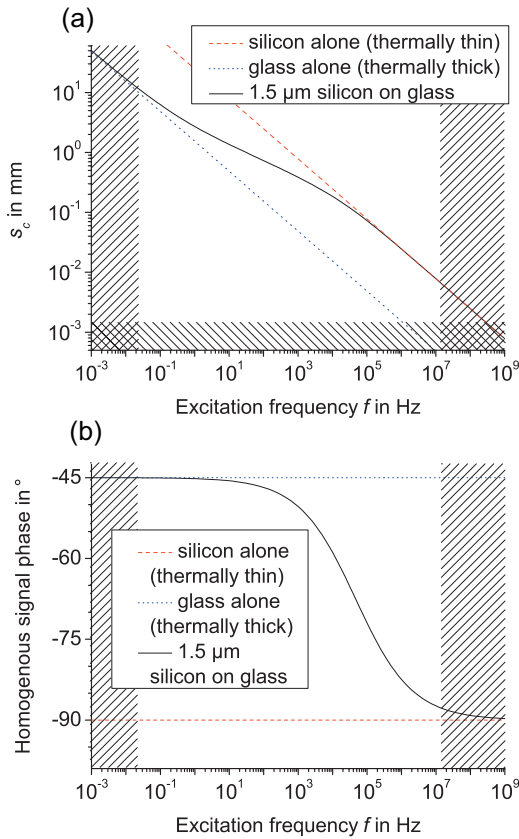


Figure 5 (online colour at: www.pss-b.com) Resolution (a) and homogeneous signal phase (b) for a CSG sample over a broad range of excitation frequencies (signal and heat source at the surface). The limiting cases thermally thin and thermally thick are plotted for comparison. The approximation of a thermally thin layer on a thermally thick substrate is invalid in the shaded regions, see text.

Resolution values taken from Fig. 5 are only valid if the assumptions made in the derivation of case (b) are still fulfilled (see the discussion in Section 3.1). For the substrate to be thermally thick it is sufficient to check if $\Lambda(f) \ll l$ at frequency $f = \omega/2\pi$. (The other sufficient condition for thermally thick behaviour $s \ll l$ can never be fulfilled for all s ranging from s_c to ∞ , that are evaluated for the resolution criterion.) For the highly heat conductive film to be thermally thin $s \gg d$ must be fulfilled down to $s_c \gg d$ as well as $\Lambda_f(f) \gg d$. These three conditions can be conveniently checked in Fig. 5 by drawing two vertical lines at the frequencies $\Lambda(f) = l$ and $\Lambda_f(f) = d$ and one horizontal line at $s_c = d$ (this is not critical in the present case). The shaded regions beyond these lines in the figure indicate values of s_c where the conditions for these approximations are clearly violated.

3.3.2 Signal phase Additional interesting information can be found from the TTF. A homogeneous source has a spatial frequency of zero. Thus, the absolute value and argument of the TTF at $k = 0$ are the amplitude (a value in K temperature modulation per Wm^{-2} heating power density)

and phase of the temperature modulation signal resulting from the excitation by a homogeneous source.

For thermally thick and thin samples this phase is known to be -45° and -90° , respectively [22]. This homogeneous signal phase is plotted in Fig. 5(b) for the silicon on glass sample described above. Note that the transition from thermally thick to thermally thin behaviour occurs at higher excitation frequencies for the homogeneous signal phase than for the resolution parameter. The reason is that the TTF is evaluated at different spatial frequencies $k = 0$ and $k = k_c$, respectively, and low spatial frequencies tend to be less influenced by the presence of the HCL.

3.3.3 Generalized plot of resolution and phase The resolution and phase information that is available through the TTF for the case of a HCL on an infinite substrate can be presented in a more general fashion than shown in Fig. 5 by summarizing all possible material combinations using appropriate dimensionless parameters.

For that, it is helpful to make a simple estimation of the ratio of heat transported laterally through the thin layer and the substrate. Consider the heat flow from a point source on top of the sample through a cylinder around this point source of a radius small compared to the thermal diffusion length in both thin layer and substrate. The heat transported through the layer to the cylinder should be proportional to its thermal conductivity λ_f and thickness d . Although the substrate is assumed to be infinitely thick, the heat will only be transported down to a depth proportional to the thermal diffusion length in the substrate Λ . The ratio v of heat transport through the layer to that through the substrate can thus be estimated as

$$v = \frac{\lambda_f d}{\lambda \Lambda} = \sqrt{\frac{\omega}{2h^2 D}} \quad (25)$$

If our estimation makes sense physically, v should be a suitable dimensionless substitute for the excitation frequency ω . To make the resulting graphs more intuitive, however, it is desirable to use a variable that is directly proportional to the frequency. Also, the factor of two should be insignificant and will be dropped to simplify the equations. We therefore define the dimensionless frequency ω' :

$$\omega' = 2v^2 = \frac{\omega}{h^2 D} \quad (26)$$

Applying Eq. (22) for the present case of a thermally thin layer on a thermally thick substrate with source and observation at the surface and substituting ω by the dimensionless ω' gives

$$\left| i\omega' \frac{D}{D_f} + \frac{k_c^2}{h^2} + \sqrt{i\omega' + \frac{k_c^2}{h^2}} \right| = \sqrt{2} \left| i\omega' \frac{D}{D_f} + \sqrt{i\omega'} \right| \quad (27)$$

The form of this equation motivates the introduction of two more dimensionless variables, the ratio of the diffusivity in

the HCL to that in the substrate D' ($D' > 1$) and the dimensionless lateral resolution k'_c , s'_c :

$$D' = \frac{D_f}{D}, \quad k'_c = \frac{k_c}{h}, \quad s'_c = \frac{2\pi}{k'_c} = h s_c. \quad (28)$$

With these substitutions (27) reads

$$\begin{aligned} & |i\omega'/D' + k'_c 2 + \sqrt{i\omega' + k'_c 2}| \\ &= \sqrt{2} |i\omega'/D' + \sqrt{i\omega'}|. \end{aligned} \quad (29)$$

The homogeneous signal phase (see Section 3.3.2) can also be expressed in these dimensionless variables, giving

$$\arg F_b(0) = \arg \left(\frac{1}{i\omega'/D' + \sqrt{i\omega'}} \right). \quad (30)$$

It is now straightforward to plot resolution and phase of every relevant system of HCL on thermally thick substrate. This plot is shown in Fig. 6.

As discussed in Section 3.3.1, care has to be taken that the highly heat conductive layer is in fact thermally thin and that the substrate is in fact thermally thick at the given frequency.

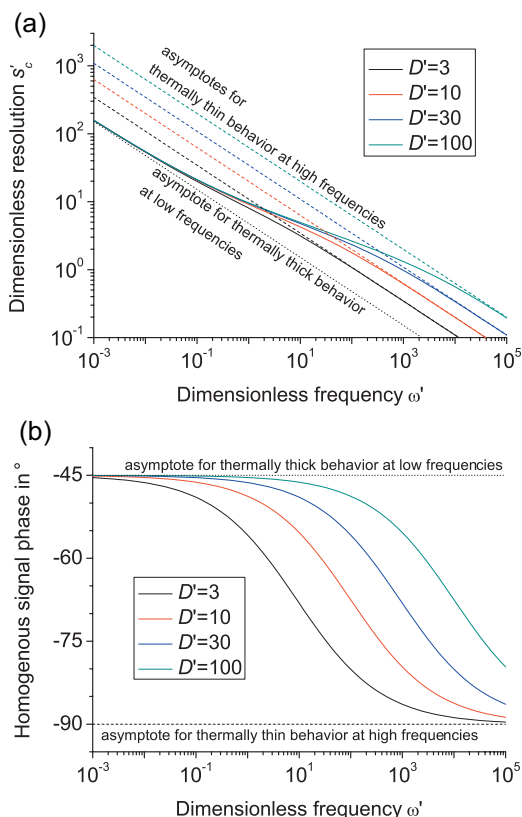


Figure 6 (online colour at: www.pss-b.com) System resolution parameter s'_c (a) and homogeneous signal phase (b) for dimensionless variables. (Signal and heat source at the surface.)

4 Experimental To confirm the theoretical calculations experimentally, three samples corresponding to the cases (a) through (c) in Fig. 1 were prepared. The corresponding LIT setup is shown schematically in Fig. 7. The surface of all samples is electrically conductive and connected to ground. A point-like heat source is realized by Joule heating at the electrical contact resistance between conductive surface and tip. The tip scratches through a layer of black spray paint applied to all samples for high and homogeneous emissivity. The samples are such that the Joule heating caused by the current flow from the tip location to ground is negligible.

Some of the heat that is generated at the contact resistance does not contribute to the thermal wave but is directly carried away by the metal tip. This does not influence the overall shape of the PSF to be measured, but introduces significant uncertainty about the amplitude of the PSF. Therefore, it is not possible to validate the constant factor of the PSF experimentally using this arrangement and the amplitude is treated as a free parameter for all measured curves.

The samples are heated by a square-wave voltage with excitation frequency f . As heating is always positive an initial heating-up phase is needed until the elevated temperature of the sample causes a heat flux to the environment which compensates the average heating through the excitation. (This does not influence the measured PSF as long as quasi-adiabatic conditions are given. This has been checked using the theory outlined in Ref. [52].) In the quasi steady state established after the initial heating-up phase is completed, the temperature variation on every point of the surface shows frequency components at f and higher harmonics due to the square-wave excitation. This variation is detected by an IR camera whose frame rate is phase-coupled to the excitation. Each frame is weighted with a sine and cosine correlation function filtering out the first harmonic (provided that more

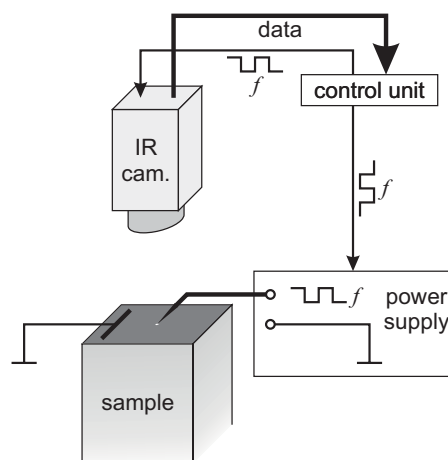


Figure 7 Setup for the measurement of the PSF. Current source, control unit and IR camera are part of Thermosensorik's TDL 640 system with an InSb detector operating in the 3–5 μm mid-range. The point-like source is realized through Joule heating at the tip contact resistance to the sample (indicated by a white spot).

than about ten frames per period are acquired). The result of the lock-in process is the amplitude and phase of the temperature variation (*i.e.*, its complex amplitude) of every point of the image of the sample. For details about the initial heating-up phase and the principle of LIT, see Ref. [22].

From the images both the PSF as well as the LSF are readily available. The PSF is found as a line-scan from the tip outwards at any angle, the LSF by integrating the image according to Eq. (12). This integration of line-scans can easily be done in an image manipulation tool and has the big advantage of using much more of the originally acquired data, thus improving the signal-to-noise ratio. We will therefore use the LSF in the following evaluations.

We will start with cases (b, thermally thick substrate with HCL) and (c, neither thermally thick nor thin sample). The theoretical complications of a HCL and a finite thickness substrate combined give case (a).

4.1 Case (b): silicon on glass The sample is a cutting taken from a practical example, a CSG solar module. For the CSG (crystalline silicon on glass) technology a layer of amorphous silicon is deposited on a 3 mm borosilicate glass substrate. This amorphous material is recrystallized in an oven for several hours to form a 1.5 μm layer of fully (poly-)crystalline material with a radial grain size of approximately 2 μm with no amorphous fraction left [65]. For this grain size and ambient temperature, the thermal properties of the material are close to the bulk silicon properties [66]. For optimal results, all further solar module processing steps (glass texturization, laser groove cutting, contacting) were left out. The measurement was performed for 2 h at a lock-in frequency of 2.9 Hz (which is well in the transition region from thermally thick to thermally thin behaviour, see Fig. 5) and with 1 V, 0.6 mA; sheet resistance $\approx 500 \Omega \square$.

Figure 8 shows the real (0°) and imaginary ($+90^\circ$) LSF of the experiment, compared to the corresponding theoretical results. The experimental curve follows the theoretical curve, only very close to the centre the shading through the heating tip itself is visible. For comparison, the thermally thick limit (only glass) and the thermally thin limit (only silicon) are also shown. The thermally thin curve needed to be scaled down by a factor of 2000 because of the low heat capacity of a 1.5 μm thin film.

4.2 Case (c): thick silicon Case (c) is important for material that is neither thin nor thick compared to the thermal diffusion length or for very high spatial frequencies in thin material. To avoid experimental difficulties connected with high resolution detection, a thick slab of silicon was chosen to test the validity of the calculations. The sample is a cutting from an experimental multicrystalline solar silicon ingot originally intended for crystal quality assessment. Its grain size is in the order of centimetre and its impurities and crystal defects do not affect the thermal properties appreciably.

The measurement was performed for 30 min at a lock-in frequency of 2.9 Hz, where the thermal diffusion length is

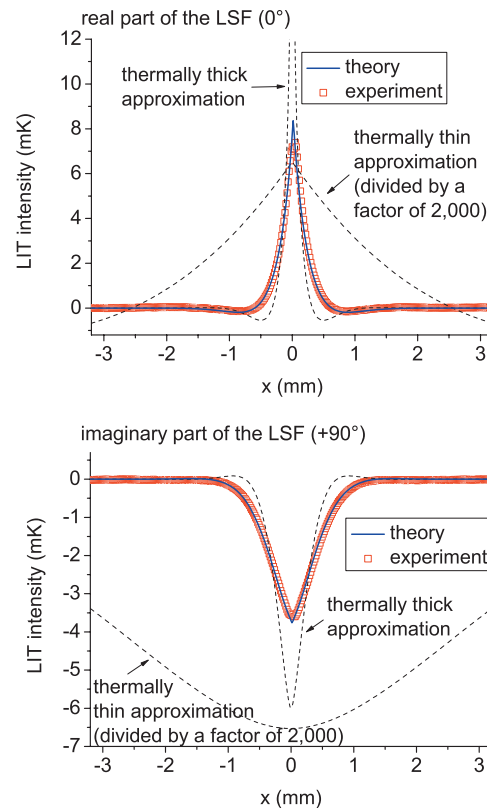


Figure 8 (online colour at: www.pss-b.com) The complex LSF of a 1.5 μm silicon film on 3 mm of glass at 2.9 Hz, compared to the theoretical limits of thermally thick heat conduction in the glass alone and thermally thin heat conduction in the silicon alone. Due to the low area heat capacity of the thin silicon layer, the resulting temperature values for this model calculation are very high (shown scaled down in the graph).

$\Lambda = 3.2 \text{ mm}$, which is neither small nor large compared to the sample thickness of $l = 2.15 \text{ mm}$. The excitation voltage and current were 19 V, 2 mA at a silicon resistivity of $\approx 1.5 \Omega \text{ cm}$.

Figure 9 shows the real (0°) and imaginary ($+90^\circ$) LSF of the experiment, compared to the corresponding theoretical results as well as the thermally thick and thin cases. Again agreement between experimental and calculated curve is excellent. A small deviation is visible in the imaginary part of the signal at a distance of 10 mm from the centre. It is due to reflections of thermal waves at the edges of the sample that was only 2.2 cm wide.

4.3 Case (a): silver on a thin glass slide This is both theoretically and experimentally the most difficult case. Therefore a specialized sample was prepared such that both the effect of the HCL and the finite thickness of the substrate are simultaneously visible. The substrate is a 1 mm thick microscope slide (2.5 cm wide) made of optical crown glass. On this substrate a layer of 200 nm silver was evaporated ($\approx 80 \text{ m}\Omega \square$).

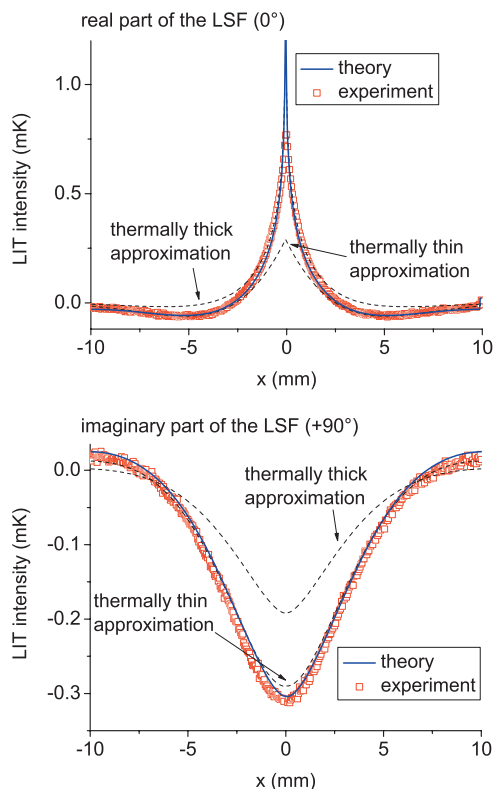


Figure 9 (online colour at: www.pss-b.com) The complex LSF of a 2.15 mm thick slab of silicon at 2.9 Hz, compared to the theoretical limits of thermally thick and thin heat conduction. Note the transition from thick to thin behaviour in the 0° -signal at increasing distances from the centre. A small deviation from theory is observed in the imaginary part of the signal due to reflections at the sample edge.

The measurement was performed for 4.5 h at a lock-in frequency of 0.06 Hz and with 0.5 V, 85 mA. Figure 10 shows the real (0°) and imaginary ($+90^\circ$) LSF of the experiment. At this very low frequency, the sample substrate is no longer thermally thick for all spatial frequency components, $\Lambda(0.06 \text{ Hz}) = 1.8 \text{ mm}$. The silver film is highly heat conductive and influences the heat conduction significantly already at $d = 200 \text{ nm}$ thickness. For comparison, the limiting cases of a thermally thin layer on a thick layer and of a single layer of finite thickness (glass) are also shown. The behaviour of the sample is clearly intermediate as expected. The real part of the signal follows the theoretical curve well. However, the imaginary part deviates significantly from theory at 5 mm from the centre, *i.e.*, in the low spatial frequency components. Our estimations show that this should be due to heat conduction from the back surface to the sample holder, which gets more effective for low spatial frequencies and at low excitation frequencies.

5 Conclusions We have solved analytically the problem of thermal wave propagation in a homogeneous slab of material with a HCL on top by using a transfer function concept. The resulting theoretical expressions were successfully tested experimentally. Also, the limits to the thermally

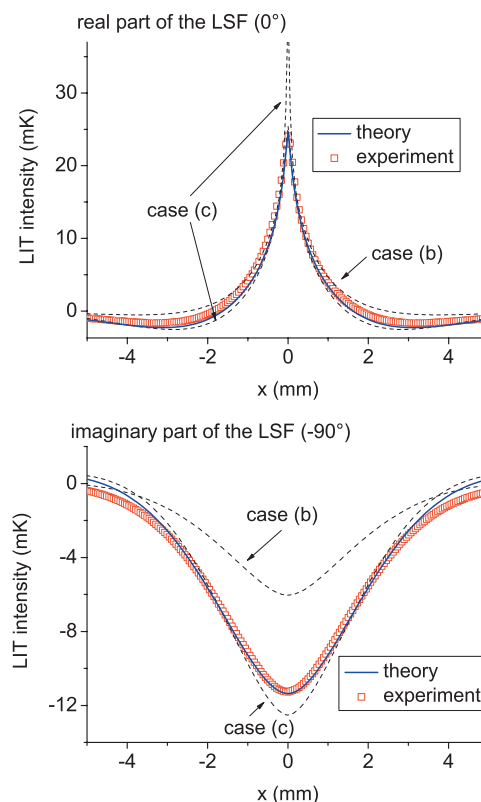


Figure 10 (online colour at: www.pss-b.com) The complex LSF of a 200 nm silver film on 1 mm of glass at 0.06 Hz, compared to cases (b) and (c).

thin and thermally thick cases give the corresponding relations widely used in the literature for LIT and photo-thermal measurement techniques.

Interestingly, the expression for a slab does not converge to the thermally thin limit if only the classical criterion is used that takes a sample to be thermally thin if it is much thinner than the thermal diffusion length in the material. That means that no real sample can in fact be thermally thin. Instead, it depends on the focus of the specific experiment (or resolution of the temperature detection) if the thermally thin approximation is valid or not. Accordingly, new definitions of the terms thermally thin and thick were proposed.

Our theoretical treatment of the heat conduction problem leads to a mathematically rigorous introduction of the complex-valued thermal transfer function, TTF, which has a much simpler mathematical form than the point or line spread function. Combined with the efficiency of numerical Fourier transforms, it is thus computationally advantageous to use the TTF to deconvolute thermal signals. Physical interpretation of the TTF as a spatial cutoff filter has led us to a resolution criterion in thermal imaging that is proposed as a replacement of the thermal diffusion length in the case of layered systems. For the specific case of a HCL on top of a thermally thick substrate, that is often found in applications, a generalized plot of resolution and phase was developed. Furthermore, the analogy to the fully developed field of

Fourier optics expressed through the TTF may lead to interesting new results for thermal wave investigations. The TTF approach developed here is directly applicable for all steady periodic heat conduction problems in radially homogeneous, layered media.

Acknowledgements The authors would like to thank Paweł Buczek and Johannes de Boor for helpful theoretical and experimental advice. This work was supported by the BMBF project SiThinSolar (contract no. 03IP607) and the BMU project SolarFocus (contract no. 0327650D).

References

- [1] H. S. Carslaw and J. C. Jaeger, *Conduction of heat in solids*, second ed. (Oxford at the Clarendon Press, Oxford, 1959).
- [2] A. Rosencwaig, *Science* **218**, 223 (1982).
- [3] A. Rosencwaig and A. Gersho, *J. Appl. Phys.* **47**, 64 (1976).
- [4] H. Vargas and L. C. M. Miranda, *Phys. Rep.* **161**, 43 (1988).
- [5] M. A. Olmstead, N. M. Amer, S. Kohn, D. Fournier, and A. C. Boccara, *Appl. Phys. A* **32**, 141 (1983).
- [6] J. Opsal, A. Rosencwaig, and D. L. Willenborg, *Appl. Opt.* **22**, 3169 (1983).
- [7] D. G. Cahill, *Rev. Sci. Instrum.* **61**, 802 (1990).
- [8] H. Wang and M. Sen, *Int. J. Heat Mass Transf.* **52**, 2102 (2009).
- [9] A. J. Schmidt, R. Cheaito, and M. Chiesa, *Rev. Sci. Instrum.* **80**, 094901 (2009).
- [10] J. Zhu, D. Tang, W. Wang, J. Liu, K. W. Holub, and R. Yang, *J. Appl. Phys.* **108**, 094315 (2010).
- [11] D. H. Hurley and K. L. Telschow, *Phys. Rev. B* **71**, 241410(R) (2005).
- [12] Y. V. Kartashov, V. A. Vysloukh, and L. Torner, *Opt. Lett.* **33**, 506 (2008).
- [13] A. O. Guimarães, M. E. Soffner, A. M. Mansanares, A. A. Coelho, A. Magnus, G. Carvalho, M. J. M. Pires, S. Gama, and E. C. da Silva, *Phys. Rev. B* **80**, 134406 (2009).
- [14] Y. H. Wong, R. L. Thomas, and G. F. Hawkins, *Appl. Phys. Lett.* **32**, 538 (1978).
- [15] J. A. Abate and R. Roides, *J. Phys. Colloq. (France)* **44**, C6/497 (1983).
- [16] K. Friedrich, K. Haupt, U. Seidel, and H. G. Walther, *J. Appl. Phys.* **72**, 3759 (1992).
- [17] A. Rosencwaig, J. Opsal, W. L. Smith, and D. L. Willenborg, *Appl. Phys. Lett.* **46**, 1013 (1985).
- [18] J. Hartmann, P. Voigt, and M. Reichling, *J. Appl. Phys.* **81**, 2966 (1997).
- [19] C. Frégnay, J. P. Roger, V. Reita, and D. Fournier, *J. Appl. Phys.* **102**, 116104 (2007).
- [20] P. K. Kuo, T. Ahmed, H. J. Jin, and R. L. Thomas, *Proc. SPIE* **1004**, 41 (1988).
- [21] G. Busse, D. Wu, and W. Karpen, *J. Appl. Phys.* **71**, 3962 (1992).
- [22] O. Breitenstein, W. Warta, and M. Langenkamp, *Lock-in thermography: Basics and use for evaluating electronic devices and materials*, second ed. (Springer, Berlin, 2010).
- [23] D. Wu and G. Busse, *Rev. Gen. Therm.* **37**, 693 (1998).
- [24] J. B. Thibaud, R. Carminati, and J. J. Greffet, *J. Appl. Phys.* **87**, 7638 (2000).
- [25] U. Werner, K. Giese, B. Sennhenn, K. Plamann, and K. Kolmel, *Phys. Med. Biol.* **37**, 21 (1992).
- [26] P. Martínez-Torres, A. Mandelis, and J. J. Alvarado-Gil, *J. Appl. Phys.* **106**, 114906 (2009).
- [27] O. Breitenstein, M. Langenkamp, F. Altmann, D. Katzer, A. Lindner, and H. Eggers, *Rev. Sci. Instrum.* **71**, 4155 (2000).
- [28] A. Mandelis (ed.), *Photoacoustic and Thermal Wave Phenomena in Semiconductors* (North-Holland, New York, 1987).
- [29] G. B. M. Fiege, A. Altes, R. Heiderhoff, and L. J. Balk, *J. Phys. D, Appl. Phys.* **32**, L13 (1999).
- [30] S. Volz (ed.), *Microscale and Nanoscale Heat Transfer* (Springer, Berlin, 2007).
- [31] T. Dehoux, O. B. Wright, R. Li Voti, and V. E. Gusev, *Phys. Rev. B* **80**, 235409 (2009).
- [32] A. Mandelis, *Diffusion-Wave Fields: Mathematical Methods and Green Functions* (Springer, New York, 2001).
- [33] A. Mandelis, L. Nicolaidis, and Y. Chen, *Phys. Rev. Lett.* **87**, 020801 (2001).
- [34] R. Li Voti, G. L. Liakhou, S. Paoloni, C. Sibilina, and M. Bertolotti, *J. Optoelectron. Adv. Mater.* **3**, 779 (2001).
- [35] C. A. Decker and T. J. Mackin, *Thin Solid Films* **473**, 196 (2005).
- [36] G. Langer, J. Hartmann, and M. Reichling, *Rev. Sci. Instrum.* **68**, 1510 (1997).
- [37] T. Borca-Tasciuc, A. R. Kumar, and G. Chen, *Rev. Sci. Instrum.* **72**, 2139 (2001).
- [38] B. Heeg and D. R. Clarke, *J. Appl. Phys.* **104**, 113119 (2008).
- [39] K. Jagannadham and H. Wang, *J. Appl. Phys.* **91**, 1224 (2002).
- [40] B. Li, L. Pottier, J. P. Roger, D. Fournier, and E. Welsch, *Rev. Sci. Instrum.* **71**, 2154 (2000).
- [41] A. J. Schmidt, R. Cheaito, and M. Chiesa, *J. Appl. Phys.* **107**, 024908 (2010).
- [42] D. G. Cahill, M. Katiyar, and J. R. Abelson, *Phys. Rev. B* **50**, 6077 (1994).
- [43] X. Liu, J. L. Feldman, D. G. Cahill, R. S. Crandall, N. Bernstein, D. M. Photiadis, M. J. Mehl, and D. A. Papaconstantopoulos, *Phys. Rev. Lett.* **102**, 035901 (2009).
- [44] H. S. Yang, D. G. Cahill, X. Liu, J. L. Feldman, R. S. Crandall, B. A. Sperling, and J. R. Abelson, *Phys. Rev. B* **81**, 104203 (2010).
- [45] Y. K. Koh and D. G. Cahill, *Phys. Rev. B* **76**, 075207 (2007).
- [46] A. A. Maznev, J. Hartmann, and M. Reichling, *J. Appl. Phys.* **78**, 5266 (1995).
- [47] K. D. Cole, *J. Heat Transfer* **128**, 709 (2006).
- [48] K. D. Cole, J. V. Beck, A. Haji-Sheikh, and B. Litkouhi, *Heat Conduction Using Green's Functions*, second ed. (CRC Press, Boca Raton, 2010).
- [49] M. Reichling and H. Grönbeck, *J. Appl. Phys.* **75**, 1914 (1994).
- [50] A. Mandelis, *J. Appl. Phys.* **78**, 647 (1995).
- [51] G. Rousset, F. Charbonnier, and L. Lepoutre, *J. Appl. Phys.* **56**, 2093 (1984).
- [52] H. Straube and O. Breitenstein, *J. Appl. Phys.* **109**, 064515 (2011).
- [53] H. K. Lyeo and D. G. Cahill, *Phys. Rev. B* **73**, 144301 (2006).
- [54] B. Davies, *Integral Transforms and Their Applications* (Springer, New York, 2002).
- [55] G. N. Watson, *A Treatise on the Theory of Bessel Functions*, second ed. (Cambridge University Press, Cambridge, 1944).
- [56] E. B. Brown, *Modern Optics*, second ed. (Reinhold Publishing Corporation, New York, 1965).

- [57] R. C. Jones, *J. Opt. Soc. Am.* **48**, 934 (1958).
- [58] E. W. Marchand, *J. Opt. Soc. Am.* **54**, 915 (1964).
- [59] W. H. Press, S. A. Teukolsky, W. T. Vetterling, and B. P. Flannery, *Numerical Recipes in C*, second ed. (Cambridge University Press, Cambridge, 1997).
- [60] S. M. Shepard, T. Ahmed, and B. C. Chaudhry, *Rev. Prog. Quant. Nondestruct. Eval.* **18**, 605 (1999).
- [61] S. M. Shepard, T. Ahmed, J. R. Lhota, and B. A. Rubadeux, *Proc. SPIE* **3993**, 14 (2000).
- [62] J.C. Krapez, Thermal modulation transfer function (TMTF), in: *Proceedings of QIRT 2000* (Reims, France, 2000), p. 162; QIRT Open Archives, <http://qirt.gel.ulaval.ca>, Paper QIRT 2000-033.
- [63] A. Mandelis, *J. Opt. Soc. Am. A* **6**, 298 (1989).
- [64] A. Salazar, A. Sánchez-Lavega, and J. M. Terrón, *J. Appl. Phys.* **84**, 3031 (1998).
- [65] M. A. Green, P. A. Basore, N. Chang, D. Clugston, R. Egan, R. Evans, D. Hogg, S. Jarnason, M. Keevers, P. Lasswell, J. O'Sullivan, U. Schubert, A. Turner, S. Wenham, and T. Young, *Sol. Energy* **77**, 857 (2004).
- [66] A. D. McConnell and K. E. Goodson, *Annu. Rev. Heat Transfer* **14**, 129 (2005).